



Superconductivity at the Polar-Nonpolar Phase Boundary of SnP with an Unusual Valence State

M. Kamitani,^{1,*} M. S. Bahramy,^{1,2} T. Nakajima,¹ C. Terakura,¹ D. Hashizume,¹ T. Arima,^{1,3} and Y. Tokura^{1,2}

¹*RIKEN Center for Emergent Matter Science (CEMS), Wako, Saitama 351-0198, Japan*

²*Department of Applied Physics, University of Tokyo, Hongo, Tokyo 113-8656, Japan*

³*Department of Advanced Materials Science, University of Tokyo, Kashiwa 277-8561, Japan*

(Received 30 April 2017; revised manuscript received 8 September 2017; published 17 November 2017)

Structural, magnetic, and electrical characterizations reveal that SnP with an unusual valence state (nominally Sn^{3+}) undergoes a ferroelectriclike structural transition from a simple NaCl-type structure to a polar tetragonal structure at approximately 250 K at ambient pressure. First-principles calculations indicate that the experimentally observed tetragonal distortion enhances the charge transfer from Sn to P, thereby making the polar tetragonal phase energetically more stable than the nonpolar cubic phase. Hydrostatic pressure is found to promptly suppress the structural phase transition in SnP, leading to the emergence of bulk superconductivity in a phase-competitive manner. These findings suggest that control of ferroelectriclike instability in a metal can be a promising way for creating novel superconductors.

DOI: 10.1103/PhysRevLett.119.207001

Ferroelectric materials are usually insulating, and yet there are some materials, known as polar metals, that possess both metallicity and ferroelectriclike distortion. In 1965, Anderson and Blount predicted the existence of a continuous structural phase transition to a ferroelectriclike state in a metal [1]. Motivated by this conjecture, materials showing polar structural transitions such as LiOsO_3 have been explored and developed [2–5]. Nevertheless, metals with polar symmetry remain scarce. Some intriguing physical properties have been confirmed experimentally in polar metals. In MoTe_2 or WTe_2 with layered structures, for instance, topologically nontrivial band structures have been observed in the polar phase [6]. Large magnetoresistance, critical enhancement of thermopower, and superconductivity under pressure coexisting with the polar phase have also been observed in these materials [7–10]. However, diversity in the physical properties arising from polar metals and controlling such properties are still to be explored.

In this study, we focus on the pressure-induced lattice- and electronic-phase change of SnP; the material itself was reported about half a century ago [11]. It is known that there is no stable phase for SnP at ambient pressure; however, a metallic rocksalt structure phase can be stabilized by a high-pressure synthesis method [12,13]. The conventional valence states of Sn in the ionic view are $2+$ or $4+$; it lacks a $3+$ valence state. Therefore, Sn is known as a valence-skipping element, analogous to Bi in BaBiO_3 [14,15], which has two nominal valence states Bi^{3+} and Bi^{5+} . The hole-doped analogs of BaBiO_3 , e.g., $\text{BaBi}_{1-x}\text{Pb}_x\text{O}_3$ [16] and $\text{Ba}_{1-x}\text{K}_x\text{BiO}_3$ [14], have been studied for a long time, because these materials seem to form a group of high- T_c superconductors. The origin of the high- T_c superconductivity has often been discussed in association with the

unique valence instability [17,18]. In this context, the nominal valence of Sn^{3+} in SnP is unusual as well. Sleight has suggested that such an unusual valence state in a rocksalt structure may be realized because of the charge frustration effect arising from the tetrahedral configuration of cations [19,20]. Although a previous work reported the coexistence of cubic and tetragonal structures at room temperature in high-pressure synthesized SnP, as well as the presence of superconductivity [11], the relation between the two structural phases and the emergence of superconductivity remains elusive. In this Letter, we show that this material is a unique example of a ferroelectriclike structural phase transition with changing temperature and/or changing external pressure. Even in the polar phase, Sn ions retain a nominal valence of $3+$. The critical temperature of the structural transition from the cubic to the tetragonal polar phase can be controlled by the hydrostatic pressure, and the superconductivity emerges when the ground-state lattice phase is turned to the cubic form. The critical temperature T_c of superconductivity as a function of the applied pressure is maximized at the critical boundary of the polar phase. These results provide unique opportunities for a further study not only on the origin of polar instability in a metallic system but also on its relation to superconductivity.

Polycrystalline samples of SnP were synthesized by using a cubic anvil-type high-pressure apparatus. Details of the synthetic procedures are given in Supplemental Material [21].

SnP can crystalize into two structures with cubic (rocksalt type; space group $Fm-3m$) and tetragonal (polar; space group $I4mm$) symmetries, as shown in Figs. 1(a) and 1(b), respectively. In the centrosymmetric cubic phase, all Sn—P bond distances are equal (2.768 Å). The tetragonal phase,

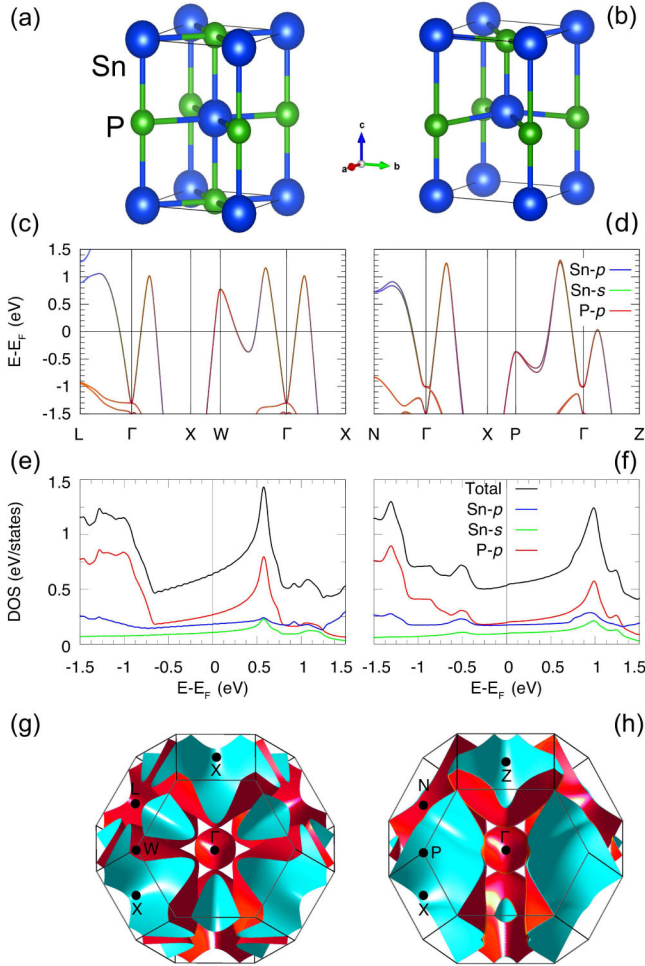


FIG. 1. Crystal structure of SnP for (a) cubic and (b) tetragonal phases. For the cubic phase, we show half of the conventional cell for clear comparison with the tetragonal phase. (c),(d) Band structure, (e),(f) density of states, and (g),(h) Fermi surfaces for cubic and tetragonal phases are shown on the left and right, respectively.

on the other hand, lacks inversion symmetry. As seen in Fig. 1(b), all the P ions appear to be equally shifted toward their adjacent Sn ions along the c axis. As a result, the Sn—P bond lengths along this direction vary between two values, 2.624 and 3.347 Å, thereby inducing a net dipolar field along the c axis [25]. Such an imbalance in the bond distances implies that the amount of charge transferred between Sn and P in the tetragonal phase is relatively different from that in the cubic phase.

To trace the nature of this difference, we show the density functional theory (DFT) band structures of the cubic and tetragonal phases in the vicinity of the Fermi level in Figs. 1(c) and 1(d), respectively. The tetragonal distortion significantly affects the energy bands along the Γ -Z direction, making them appear at relatively lower energies as compared to bands crossing the Fermi level along the Γ -X direction in the cubic phase. The affected bands are all dominated by P- p orbitals. This accordingly

means that, upon the tetragonal phase transition, the P ions gain more electrons. A comparison between the orbital projected density of states (DOS) for the cubic phase [Fig. 1(e)] and that for the tetragonal phase [Fig. 1(f)] clearly indicates that in the latter the states made of P- p orbitals are overall at relatively lower energies as compared with the same states in the cubic phase [see Fig. S3(b) in Supplemental Material [21]]. As a result, the P- p orbitals in the tetragonal phase can more effectively hybridize with their neighboring Sn- p counterparts, which energetically spread down to 6 eV below the Fermi level [see Fig. S3(a) in Supplemental Material [21]]. Such hybridization in turn lowers the total energy of the tetragonal phase, making it more stable than the cubic phase. To quantify this, we calculated the free energy for both phases. Our calculations indicated that the tetragonal phase energetically lies below the cubic phase by 54 meV per formula unit. This is consistent with the observation that SnP prefers the tetragonal phase at low temperatures, as will be discussed later. The tetragonal distortion also modifies the shape of the Fermi pockets, as shown in Figs. 1(g) and 1(h). In the cubic phase, in addition to a small electron pocket centered at the Γ point, there exist six hole pockets. A small Fermi sheet is seen between each pair of hole pockets, resulting from the energy valleys formed by the conduction and valence bands at the Fermi level. Upon the phase transition, the Fermi pockets encompassing the lateral square faces merge with the small adjacent pockets above and below them, together forming four large sheets (eight if spin splitting is included) elongated along the k_z direction.

To clarify the structural property in SnP, the temperature dependence of powder x-ray diffraction (XRD) profiles was measured during the cooling process down to 5 K [Fig. 2(a)]. At room temperature, only the XRD peaks from the cubic structure are observed. With decreasing temperature, new XRD peaks appear from the tetragonal phase below 240 K. XRD peaks from the cubic phase become weaker with decreasing temperature, whereas those from the tetragonal phase become stronger without appreciably changing the respective XRD angles. The XRD peaks from the residual cubic phase are discerned even at 5 K. The temperature dependence of the molar fractions of the respective structural phases is shown in Fig. 2(b). At the lowest temperature, the cubic phase remains with a molar fraction of approximately 0.13.

Figure 2(c) shows the temperature dependence of the magnetic susceptibility (χ). SnP shows a diamagnetic response for the whole temperature region measured, perhaps overlapped with Pauli paramagnetism. A large thermal hysteresis corresponding to the structural transition is discerned for the cooling and warming processes. For the cooling process, the magnetic susceptibility increases with the cubic-to-tetragonal structural transition. This cannot be accounted for by the change of Pauli paramagnetic susceptibility that is proportional to the DOS at the Fermi

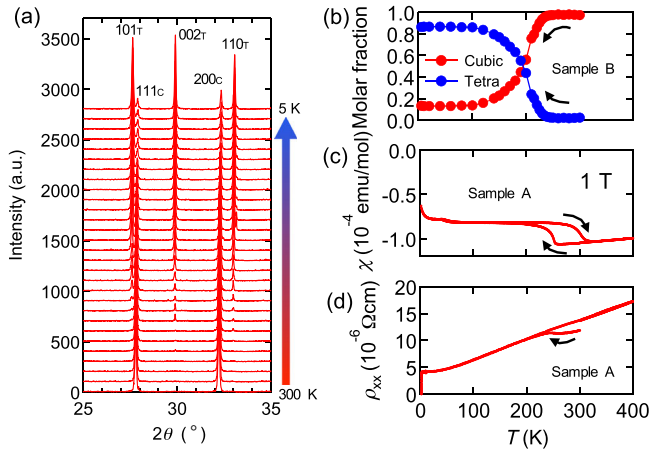


FIG. 2. (a) Powder x-ray diffraction profiles for SnP (sample *B*; see the experimental details in Supplemental Material [21]) from 300 to 5 K. (b) Temperature dependence of the molar fraction of cubic (red circles) and polar tetragonal (blue circles) phases for sample *B*. (c) Temperature dependence of the magnetic susceptibility for sample *A* under a magnetic field of 1 T. (d) Temperature dependence of the resistivity for sample *A*. Black arrows indicate the directions of the temperature scans.

level; the DFT results indicate the decrease of DOS at the Fermi level upon the cubic-to-tetragonal structural transition. The Rashba-type spin splitting of the conduction bands in the polar phase may contribute to orbital paramagnetism in a nontrivial manner [26].

The temperature dependence of resistivity is shown in Fig. 2(d). Upon decreasing the temperature from 300 K, a resistivity upturn is observed at approximately 250 K, which is thought to reflect the depletion of DOS at E_F upon the structural phase transition. A resistivity drop due to the minor superconducting phase is observed below 5 K (we will describe the superconducting properties later in detail). In the warming process, however, there is no anomaly corresponding to the structural transition back to the cubic phase, although it is apparently seen in the temperature dependence of χ .

It is to be noted here that the structural phase transition temperature (T_s) and its hysteretic behavior as probed by these physical properties strongly depend on the sample condition. The hysteretic behavior in the magnetic susceptibility [Fig. 2(c)] appears to be completed at 180–200 K, i.e., at the lower-temperature side, whereas the structural data [Fig. 2(b)] indicate the more robust coexistence of the high-temperature cubic phase, e.g., the change in the volume fraction seen down to below 100 K and the subsisting minor fraction of the cubic phase even at the lowest temperature (5 K). This difference is not simply due to the different sensitivities of the respective probes but perhaps mainly to the residual strain effect and/or finite-size grain effect of the finely ground sample for the XRD measurement; the phase transition is extremely sensitive to the applied pressure, as shown below, and hence perhaps to

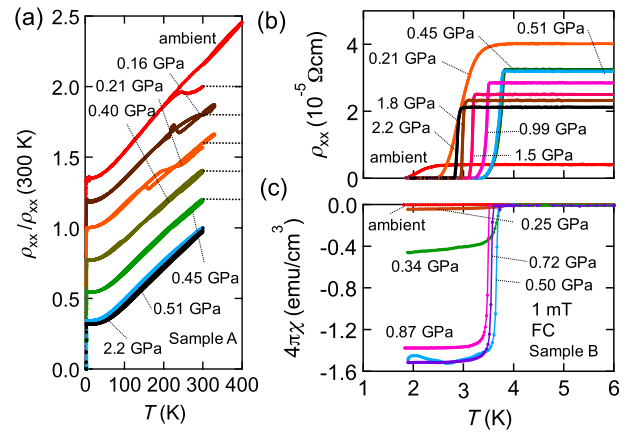


FIG. 3. (a) Temperature dependence of the resistivity under hydrostatic pressure normalized by the value at 300 K (sample *A*). The data are vertically offset by -0.2 at every pressure value for clarity. (b) Temperature dependence of the resistivity under hydrostatic pressure at a low-temperature region for sample *A*. (c) Temperature dependence of the magnetic susceptibility under hydrostatic pressure in the field-cooling process with a magnetic field of 1 mT for sample *B*.

the residual strains in the microcrystalline grains. As another example, the densely pressurized pellet sample (sample *B*, described in Table S1 in Supplemental Material [21]) composed of small crystals (approximately several tens of microns in size) was broken into pieces during multiple temperature scans at ambient pressure.

Figure 3(a) shows the temperature dependence of the resistivity normalized by the value at 300 K under various hydrostatic pressures. Metallic temperature dependence is discerned for the whole pressure region investigated. In the low-pressure region, the first-order phase transition goes down to the low-temperature region with increasing pressure up to 0.4 GPa. At 0.45 GPa, there is no thermal hysteresis corresponding to the lattice phase transition. Thus, the tetragonal polar phase in SnP is suppressed and disappears at pressures above 0.45 GPa. Because the cell volume of the tetragonal phase is larger than that of the cubic phase (see Fig. S5 in Supplemental Material [21]), the cubic phase is favored at high pressure.

Let us turn our attention to the low-temperature region [see Fig. 3(b)]. At ambient pressure, the resistivity decreases below 2.5 K because of the occurrence of a superconducting transition and gradually reaches zero down to 1.8 K. With increasing pressure, a sharp drop in resistivity occurs at a higher temperature. The highest superconducting transition temperature (3.4 K) is observed at 0.45 GPa, where the lattice phase transition to the polar phase is completely suppressed. However, a further increase of pressure reduces the superconducting transition temperature gradually, e.g., to 2.8 K at 2.2 GPa. Figure 3(c) shows the temperature dependence of the magnetic susceptibility at a small magnetic field (1 mT) in the cooling process, pointing to the Meissner signal in the

superconducting state. The overall results of the Meissner signals are in good accordance with the results of resistivity, whereas the resistivity drop in the low-pressure (<0.4 GPa) polar phase never manifests bulk superconductivity in the Meissner signal. The superconducting volume fraction appears quite low at the low-pressure region, i.e., in the polar phase region (approximately 0.1% and 4% at ambient pressure and 0.25 GPa, respectively), suggesting its filamentary character. In particular, the gradual resistivity drop observed at ambient pressure originates from the residual cubic phase in the sample composed of fine-microcrystalline grains (sample A). By contrast, clear Meissner signals are confirmed above 0.50 GPa, indicating that the bulk superconductivity emerges when the cubic phase is stabilized down to the lowest temperature. This is apparently different from the pressure effect on superconductivity in MoTe_2 , where the “bulk” superconducting phase and the polar phase coexist [9,10]. The apparent superconducting volume fraction exceeds the value of 100% above 0.50 GPa, which may be ascribed to the finite demagnetization factor [27–29].

On the basis of the transport and magnetic measurements under pressure, the electronic phase diagram for SnP is presented in the plane of pressure vs temperature [Fig. 4(b)]. The first-order phase transition from the cubic phase to the polar tetragonal phase is gradually suppressed by pressures up to 0.4 GPa. A domelike T_c curve is obtained as a function of the pressure. The superconducting transition temperature (T_c) reaches a maximum at 0.45 GPa, where the structural phase boundary is located, with a steep increase of the Meissner signal magnitude around the critical pressure [see Fig. 4(a)]. Even though superconductivity emerges at a higher pressure region away from the structural phase boundary, T_c monotonically decreases with increasing pressure [30]. Our observation strongly suggests that ferroelectriclike instability and superconductivity are closely correlated with each other.

Here, let us discuss the origin of superconductivity in SnP. The T_c is observed to decrease with making the system away from the structural phase boundary. It is occasionally observed that structural instability induces the superconducting phase or enhances the superconducting transition temperature in the vicinity of the structural phase boundary; such a feature has been observed, for example, in doped BaNi_2As_2 [32], doped or intercalated IrTe_2 [33–35], and tellurium under high pressure [36]. Enhancement of the electron-phonon coupling near the structural phase boundary is a possible origin of superconductivity in these materials. There is, however, another interesting scenario for superconductivity in incipient-ferroelectric or quantum-paraelectric systems such as slightly electron-doped SrTiO_3 or KTaO_3 [37–39], where the ferroelectric fluctuation or softened optical phonon modes may be anticipated to contribute to the s -wave pairing [40]. Although the polar-to-nonpolar structural transition in SnP appears to be strongly of a first-order nature, the present first-principles calculation based on the experimentally obtained lattice parameters

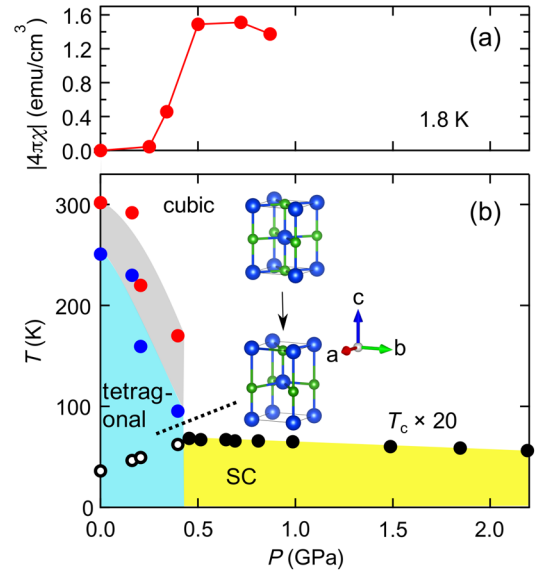


FIG. 4. (a) Pressure dependence of the magnitude of the magnetic susceptibility (Meissner signal) at 1.8 K. (b) Electronic and lattice phase diagram of SnP in the plane of pressure and temperature. Red and blue circles indicate the cubic (nonpolar)–tetragonal (polar) transition temperature T_s observed in the warming and cooling processes, respectively. Only T_s at ambient pressure is determined from the magnetic susceptibility measurement. The open circles represent the superconducting transition temperature with a filamentary (not bulk) component. The superconductivity of the bulk nature, where T_c is plotted with solid circles, was identified from the superconducting fraction of the Meissner signal combined with the resistivity data. T_c was determined from the value of zero resistivity. We plotted T_c multiplied by 20 for clarity.

predicts that the $\mathbf{q} = 0$ optical phonon mode is appreciably softened from 25 to 17 meV upon the tetragonal-to-cubic transition (see Fig. S4 in Supplemental Material [21] for the phonon dispersions in both phases). The softened optical mode may gain a larger electron-phonon (e -ph) coupling to contribute to the pairing [41,42]. To quantify this, we calculated the e -ph coupling (λ) and the superconducting T_c value for cubic and tetragonal phases of SnP using the Migdal-Eliashberg theory [43,44]. The calculation suggests that λ in the cubic phase is approximately 0.47, roughly 1.5 times larger than that obtained for the tetragonal phase. In addition, the increase of the DOS at the Fermi level upon the polar-to-nonpolar lattice transition by approximately 18% [see Figs. 1(e) and 1(f)] may contribute to the higher T_c as well. The estimated T_c obtained for the cubic and tetragonal phases is approximately 2.5 and 0.15 K, respectively, in reasonably good agreement with the experimental values described above. On the other hand, the fact that the superconducting dome does not diminish, even in the far region away from the structural phase boundary, suggests that phonon softening seems to play a subsidiary role for superconductivity.

In conclusion, we have clarified the first-order structural phase transition from the cubic to the ferroelectriclike tetragonal structure in SnP with an unusual valence state and also the emergence of superconductivity upon the pressure suppression of the structural transition. First-principles calculations reveal that the polar-tetragonal phase is stabilized because of the enhancement of charge transfer from Sn to P. The tetragonal polar phase is stable at ambient pressure, but, by applying pressure as low as 0.5 GPa, the cubic phase is immediately stabilized and bulk superconductivity emerges at the critical boundary with the ferroelectriclike phase in a phase-competitive manner. Matthias conjectured that ferroelectricity and superconductivity compete with each other, which was later supported by theoretical calculations [45,46]. Our results seem to support this scenario.

We thank Y. Taguchi, M. Kriener, R. Arita, and T. Koretsune for fruitful discussions and comments. This work was partly supported by Grants-In-Aid for Scientific Research (Grant No. 24224009) from the MEXT of Japan.

*manabu.kamitani@riken.jp

- [1] P. W. Anderson and E. I. Blount, *Phys. Rev. Lett.* **14**, 217 (1965).
- [2] Y. Shi, Y. Guo, X. Wang, A. J. Princep, D. Khalyavi, P. Manuel, Y. Michiue, A. Sato, K. Tsuda, S. Yu, M. Arai, Y. Shirako, M. Akaogi, N. Wang, K. Yamaura, and A. T. Boothroyd, *Nat. Mater.* **12**, 1024 (2013).
- [3] T. H. Kim, D. Puggioni, Y. Yuan, L. Xie, H. Zhou, N. Campbell, P. J. Ryan, Y. Choi, J.-W. Kim, J. R. Patzner, S. Ryu, J. P. Podkaminer, J. Irwin, Y. Ma, C. J. Fennie, M. S. Rzechowski, X. Q. Pan, V. Gopalan, J. M. Rondinelli, and C. B. Eom, *Nature (London)* **533**, 68 (2016).
- [4] I. A. Sergienko, V. Keppens, M. McGuire, R. Jin, J. He, S. H. Curnoe, B. C. Sales, P. Blaha, D. J. Singh, K. Schwarz, and D. Mandrus, *Phys. Rev. Lett.* **92**, 065501 (2004).
- [5] K. Ohgushi, J. I. Yamaura, M. Ichihara, Y. Kiuchi, T. Tayama, T. Sakakibara, H. Gotou, T. Yagi, and Y. Ueda, *Phys. Rev. B* **83**, 125103 (2011).
- [6] I. Belopolski, D. S. Sanchez, Y. Ishida, X. Pan, P. Yu, S.-Y. Xu, G. Chang, T. Chang, H. Zheng, N. Alidoust, G. Bian, M. Neupane, S.-M. Huang, C.-C. Lee, Y. Song, H. Bu, G. Wang, S. Li, G. Eda, H.-T. Jenget *al.*, *Nat. Commun.* **7**, 13643 (2016).
- [7] M. N. Ali, J. Xiong, S. Flynn, J. Tao, Q. D. Gibson, L. M. Schoop, T. Liang, N. Haldolaarachchige, M. Hirschberger, N. P. Ong, and R. J. Cava, *Nature (London)* **514**, 205 (2014).
- [8] H. Sakai, K. Ikeura, M. S. Bahramy, N. Ogawa, D. Hashizume, J. Fujioka, Y. Tokura, and S. Ishiwata, *Sci. Adv.* **2**, e1601378 (2016).
- [9] Y. Qi, P. G. Naumov, M. N. Ali, C. R. Rajamathi, W. Schnelle, O. Barkalov, M. Hanfland, S.-C. Wu, C. Shekhar, Y. Sun, V. Stüß, M. Schmidt, U. Schwarz, E. Pippel, P. Werner, R. Hillebrand, T. Frster, E. Kampert, S. Parkin, R. J. Cava, C. Felser, B. Yan, and S. A. Medvedev, *Nat. Commun.* **7**, 11038 (2016).
- [10] H.-J. Kim, S.-H. Kang, I. Hamada, and Y.-W. Son, *Phys. Rev. B* **95**, 180101 (2017).
- [11] P. C. Donohue, *Inorg. Chem.* **9**, 335 (1970).
- [12] O. Olofsson, *Acta Chem. Scand.* **24**, 1153 (1970).
- [13] V. Tallapally, R. J. A. Esteves, L. Nahar, and I. U. Arachchige, *Chem. Mater.* **28**, 5406 (2016).
- [14] R. J. Cava, B. Batlogg, J. J. Krajewski, R. Farrow, L. W. Rupp Jr, A. E. White, K. Short, W. F. Peck, and T. Kometani, *Nature (London)* **332**, 814 (1988).
- [15] S. Pei, J. D. Jorgensen, B. Dabrowski, D. G. Hinks, D. R. Richards, A. W. Mitchell, J. M. Newsam, S. K. Sinha, D. Vaknin, and A. J. Jacobson, *Phys. Rev. B* **41**, 4126 (1990).
- [16] A. W. Sleight, J. L. Gillson, and P. E. Bierstedt, *Solid State Commun.* **17**, 27 (1975).
- [17] C. M. Varma, *Phys. Rev. Lett.* **61**, 2713 (1988).
- [18] R. Mincas, J. Ranninger, and S. Robaszkiewicz, *Rev. Mod. Phys.* **62**, 113 (1990).
- [19] A. W. Sleight, *Prog. Solid State Chem.* **37**, 251 (2009).
- [20] Y. Wang, H. Sato, Y. Toda, S. Ueda, H. Hiramatsu, and H. Hosono, *Chem. Mater.* **26**, 7209 (2014).
- [21] See Supplemental Material at <http://link.aps.org/supplemental/10.1103/PhysRevLett.119.207001> for the details of experimental and theoretical methods, notes on the impurity phase of pure Sn, additional data for density of states, phonon dispersions, the temperature dependence of cell volume, and Refs. [22–24].
- [22] F. Izumi and K. Momma, *Solid State Phenom.* **130**, 15 (2007).
- [23] P. Blaha, K. Schwarz, G. Madsen, D. Kvasnicka, and J. Luitz, WIEN2k package, <http://www.wien2k.at>.
- [24] P. Giannozzi, S. Baroni, N. Bonini, M. Calandra, R. Car, C. Cavazzoni, D. Ceresoli, G. L. Chiarotti, M. Cococcioni, I. Dabo, A. Dal Corso, S. de Gironcoli, S. Fabris, G. Fratesi, R. Gebauer, U. Gerstmann, C. Gougoussis, A. Kokalj, M. Lazzeri, L. Martin-Samoset *al.*, *J. Phys. Condens. Matter* **21**, 395502 (2009).
- [25] See Fig. S5 in Supplemental Material [21] for the temperature dependence of the Sn—P bond length along the *c* axis.
- [26] G. A. H. Schober, H. Murakawa, M. S. Bahramy, R. Arita, Y. Kaneko, Y. Tokura, and N. Nagaosa, *Phys. Rev. Lett.* **108**, 247208 (2012).
- [27] B. Keimer, I. A. Aksay, J. Bossy, P. Bourges, H. F. Fong, D. L. Milius, L. P. Regnault, D. Reznik, and C. Vettier, *Physica (Amsterdam)* **234–236B**, 821 (1997).
- [28] Z. Ren, M. Kriener, A. A. Taskin, S. Sasaki, K. Segawa, and Y. Ando, *Phys. Rev. B* **87**, 064512 (2013).
- [29] If a proper demagnetization factor, e.g., $\sim 1/3$ for the spheric shape of the sample, is assumed, the observed Meissner signal magnitude well ensures the bulk nature of the superconductivity above 0.5 GPa.
- [30] Such a domelike pressure dependence of T_c combined with the low T_c value at ambient pressure excludes the possibility of a superconducting transition from possible impurity-phase Sn in our sample (see also Ref. [31] and the discussion in Supplemental Material [21]).
- [31] L. D. Jennings and C. A. Swenson, *Phys. Rev.* **112**, 31 (1958).
- [32] K. Kudo, M. Takasuga, Y. Okamoto, Z. Hiroi, and M. Nohara, *Phys. Rev. Lett.* **109**, 097002 (2012).

- [33] J. J. Yang, Y. J. Choi, Y. S. Oh, A. Hogan, Y. Horibe, K. Kim, B. I. Min, and S-W. Cheong, *Phys. Rev. Lett.* **108**, 116402 (2012).
- [34] S. Pyon, K. Kudo, and M. Nohara, *J. Phys. Soc. Jpn.* **81**, 053701 (2012).
- [35] M. Kamitani, M. S. Bahramy, R. Arita, S. Seki, T. Arima, Y. Tokura, and S. Ishiwata, *Phys. Rev. B* **87**, 180501(R) (2013).
- [36] F. Mauri, O. Zakharov, S. de Gironcoli, S. G. Louie, and M. L. Cohen, *Phys. Rev. Lett.* **77**, 1151 (1996).
- [37] A. G. Swartz, H. Inoue, T. A. Merz, Y. Hikita, S. Raghu, T. P. Devereaux, S. Johnston, and H. Y. Hwang, [arXiv:1608.05621v2](https://arxiv.org/abs/1608.05621v2).
- [38] S. E. Rowley, L. J. Spalek, R. P. Smith, M. P. M. Dean, M. Itoh, J. F. Scott, G. G. Lonzarich, and S. S. Saxena, *Nat. Phys.* **10**, 367 (2014).
- [39] K. Ueno, S. Nakamura, H. Shomotani, H. T. Yuan, N. Kimura, T. Nojima, H. Aoki, Y. Iwasa, and M. Kawasaki, *Nat. Nanotechnol.* **6**, 408 (2011).
- [40] J. M. Edge, Y. Kedem, U. Aschauer, N. A. Spaldin, and A. V. Balatsky, *Phys. Rev. Lett.* **115**, 247002 (2015).
- [41] M. Hoesch, T. Fukuda, J. Mizuki, T. Takenouchi, H. Kawarada, J. P. Sutter, S. Tsutsui, A. Q. R. Baron, M. Nagao, and Y. Takano, *Phys. Rev. B* **75**, 140508(R) (2007).
- [42] C. Tang, C. Liu, G. Zhou, F. Li, H. Ding, Z. Li, D. Zhang, Z. Li, C. Song, S. Ji, K. He, L. Wang, X. Ma, and Q.-K. Xue, *Phys. Rev. B* **93**, 020507(R) (2016).
- [43] A. B. Migdal, *Sov. Phys. JETP* **34**, 996 (1958).
- [44] G. M. Eliashberg, *Sov. Phys. JETP* **11**, 696 (1960).
- [45] B. T. Matthias, *Mater. Res. Bull.* **5**, 665 (1970).
- [46] Y. Krivolapov, A. Mann, and J. L. Birman, *Phys. Rev. B* **75**, 092503 (2007).